Dalton Transactions

ROYAL SOCIETY OF CHEMISTRY

COMMUNICATION

View Article Online
View Journal | View Issue

Cite this: *Dalton Trans.*, 2024, **53**, 6162

Received 13th January 2024,
Accepted 23rd February 2024

DOI: 10.1039/d4dt00108g

rsc.li/dalton

The mechanism governing the formation of intermolecular charge transfer bands: a series of polyoxomolybdates as a case study†

Xiao-Yue Zhang, Jin-Ai Fan, Zhe-Hong Chen, Cai Sun * and Shou-Tian Zheng *

A series of proof-of-concept models of polyoxomolybdates with different protonated disubstituted aniline counterions and the same β-Mo_8O_{26} polyanion were synthesized to study the mechanism governing the formation of the intermolecular charge transfer (inter-CT) band.

Charge transfer (CT) bands are a characteristic feature of the spectra of many compounds, and they signify a transfer of charge from one atomic or molecular orbital to another after excitation by light, and are usually located in the ultraviolet (UV) or visible region.[1] In contrast to the spin-allowed and Laporte-forbidden d–d transitions, CT transitions are spin-allowed and Laporte-allowed, and therefore, their molar absorption coefficient (ε) is strong, with ε as high as 10^4–10^5 L mol^{-1} cm^{-1}, which is 100–1000 times greater than that of the d–d transition.[2]

There has been a great deal of research in the fields of photoelectric detection,[3] and photoelectric[4] and photothermal conversion[5] to design and synthesize new compounds whose CT bands cover the entire visible region and even extend into the infrared (IR) region. Intramolecular charge transfer (intra-CT),[6] such as that in organic molecules with 'push–pull' electronic structure characteristics, has been extensively studied,[7] as well as metal complexes with intervalence charge transfer (IVCT),[8,9] ligand-to-ligand charge transfer (LLCT),[10] metal-to-ligand charge transfer (MLCT),[11] and ligand-to-metal charge transfer (LMCT).[12,13] In contrast, the study of inter-CT has been neglected for a long time. It is a great challenge to reveal the essence of inter-CT absorption bands and realize broadening inter-CT bands.

Polyoxometalates (POMs) were selected for further examination for the following reasons. First, POMs are commonly used in the dehydration and condensation of inorganic oxygenates with d^0 metal centers, such as V, Nb, Ta, Mo, and W, to form multinuclear metal-oxo clusters.[14–17] It has been determined that the polyanion clusters in POMs are an excellent class of electron acceptor molecules, capable of storing multiple electrons, known as electron sponges, and they also have the ability to promote the concentration of charge and interact with planar-conjugated organic electron donors.[18–20] When interacting with organic electron donors, a charge-transfer polyoxometalate (CTP) is often formed. Second, the polyanions within POMs inherently exhibit LMCT from non-bonding electrons on oxo ligands to the empty d orbitals of a metal center.[21–23] For example, the LMCT occurs in the UV region for the polyanion of polyoxomolybdate (POMo), without absorbance in the visible region,[24,25] which lays robust groundwork for clearly investigating the inter-CT bands.

Here, a series of proof-of-concept models of POMos, consisting of different protonated disubstituted aniline counterions and the same β-Mo_8O_{26} polyanion, were designed and synthesized to determine the reason why the inter-CT band forms (Fig. 1). Three representative examples of POMos were identified from the Cambridge Crystallographic Data Center (CCDC) database: $(Hopda)_4[\beta\text{-}Mo_8O_{26}]\cdot 2H_2O$ (**1**, opda = *o*-phenylenediamine), $(H_2mpda)_2[\beta\text{-}Mo_8O_{26}]\cdot 4H_2O$ (**2**, mpda = *m*-phenylenediamine), and $(H_2ppda)_2[\beta\text{-}Mo_8O_{26}]\cdot 6H_2O$ (**3**, ppda = *p*-phenylenediamine). Interestingly, **1** exhibits clear inter-CT bands ranging from 400 to 1200 nm, whereas **2** and **3** do not.

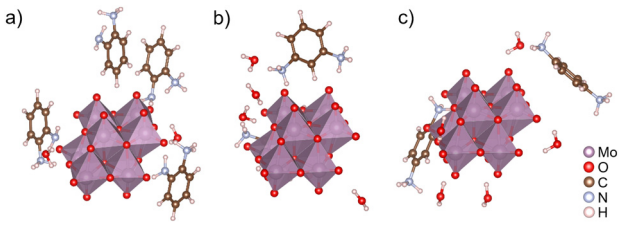

Fig. 1 Molecular structure of (a) **1**, (b) **2**, and (c) **3**.

Fujian Provincial Key Laboratory of Advanced Inorganic Oxygenated Materials, College of Chemistry, Fuzhou University, Fuzhou 350108, Fujian, China. E-mail: csun@fzu.edu.cn, stzheng@fzu.edu.cn

†Electronic supplementary information (ESI) available. See DOI: https://doi.org/10.1039/d4dt00108g

POMo **1**, **2**, and **3** were synthesized according to a protocol from a previous study.[26] Powder X-ray diffraction was used to determine the purity of the samples (Fig. S1†). The molecular structures of POMo **1**, **2**, and **3** contain one isolated β-Mo_8O_{26} polyanion (Mo_8). The polyanion is composed of eight edge-sharing MoO_6 octahedra, forming a centrosymmetric parallelepiped-shaped cluster with eight Mo atoms positioned at the vertexes. The counterions of these three POMos are aniline

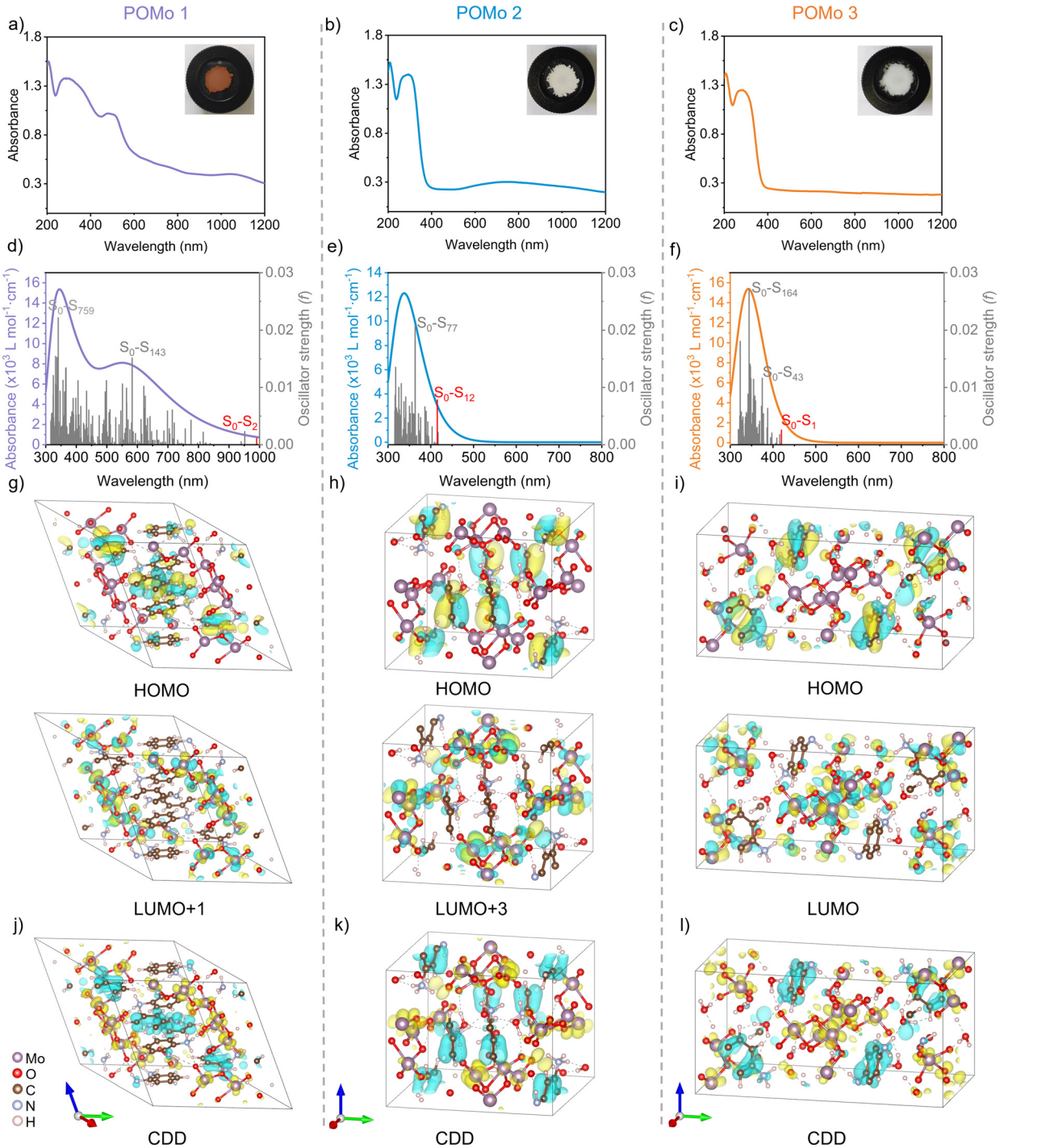

Fig. 2 UV-vis absorption spectra of (a) **1**, (b) **2**, and (c) **3**; inset: the colors of the compounds. Simulated UV-vis absorption spectra (curve) and oscillator strength (gray spikes; the main oscillator strength in the initial excited state is marked red) of (d) **1**, (e) **2**, and (f) **3**. Spatial distributions of the HOMO and LUMO+1 for (g) **1**, (h) HOMO and LUMO+3 for **2**, and (i) HOMO and LUMO for **3**. Charge density difference between (j) **1**, (k) **2**, and (l) **3**; the yellow and blue colors represent the charge accumulation and depletion upon charge transfer, respectively, with an iso-surface value of 0.001 e·Å^{-3}. Crystal axis: a, red; b, green; c, blue.

molecules with different disubstituted patterns. Notably, **1** contains four mono-protonated opda cations (Hopda), and compounds **2** and **3** contains two di-protonated mpda (H_2mpda) and two di-protonated ppda cations (H_2ppda), respectively.

As shown in Fig. 2, only **1** appears orange-red, while **2** and **3** appear white in colour. To investigate the cause of the abnormal colour of **1**, we performed UV-vis absorption spectroscopy (Fig. 2a). It was found that **1** exhibited a distinct absorption band at 400–600 nm with a midpoint at 493 nm, and a broad absorption band at 600–1200 nm, which were consistent with the observed colour. In contrast, there was nearly no absorption in the visible region for **2** and **3** (Fig. 2b and c).

To investigate the origin of the absorption band in the visible region of **1**, the UV-vis absorption spectra of aqueous solutions of the three anilines were tested (Fig. S2†). The results showed that there was no absorbance in the visible region for the anilines, and they assumed a colorless state. Given the protonated disubstituted aniline in these POMos, the absorption spectra of $Hopda^+$ and H_2opda^{2+} (Fig. S3†) were obtained, and no absorbance in the visible region was observed. Thus, the absorption band in the visible region of **1** does not originate from inherent aniline absorption. Previous studies have reported that the LMCT of polyanions in POMo occurs in the UV region.[24,25] Therefore, the absorption band in the visible region of **1** arises from inter-CT.

The crystallographic data show that the shortest distances between the ammonium counterion and polyanion in **1**, **2**, and **3** are 1.978 Å, 1.816 Å, and 1.759 Å (Fig. S4†), respectively. Similar intermolecular distances indicate that the inter-CT absorption of **1** is not primarily caused by intermolecular distance. To understand why inter-CT occurs, time-dependent density functional theory (TD-DFT) calculations were conducted to simulate the electronic absorption spectra of POMos **1**.[27] The number of calculated excited states was 1000, which adequately covers the wavelength range of 300–1000 nm for **1**. The simulated absorption spectrum (Fig. 2d) is closely aligned with the experimental spectrum (Fig. 2a).

The excited state with low energy as well as all excited states with oscillator strengths greater than 0.01 were selected for a detailed analysis (Table 1). In spectroscopy, oscillator strength is a dimensionless quantity that expresses the probability of absorption or emission of electromagnetic radiation in transitions between the energy levels of an atom or molecule.[28] The electronic transition % indicates the contribution of each orbital transition to an excited state. The transition wavelength from the ground state to the second excited state (S_0–S_2) in **1** is 990.49 nm, with oscillator strength of 0.00109, which is contributed by HOMO to LUMO+1 (100%). The frontier molecular orbital data for **1** (Fig. 2g and Fig. S5b, c†) indicates that the HOMO predominantly resides on the conjugated p–π orbitals between the aromatic ring and the N-atoms of the $-NH_2$ group, while the LUMO+1 is primarily situated on the Mo atoms within the polyanion. This indicates that Hopda tends to provide electrons, while polyanions tend to accept electrons.[29]

An excited state can be described as a hole and electron, where charge is transferred from the hole to the electron. The hole–electron analysis (Fig. S8†) of the excited states S_0–S_2 of **1** show that the holes are mainly distributed on the Hopda, and the electrons are primarily situated on the polyanion. The decrease in the charge density on the Hopda and the increase in the charge density on the polyanion are clearly seen when examining the charge density difference (CDD) maps (Fig. 2j and Fig. S5d†), which proves that S_0–S_2 is a component of the inter-CT from Hopda to polyanion. According to the calculated hole, electron, and CDD map (see the Appendix in the ESI†), for other excited states, the inter-CT bands can range from 331.66 to 990.49 nm. The results also indicate that there are other charge transfer types in POMo **1**. The polyanions inherently exhibit LMCT from oxo ligands to the Mo, which primarily appears at the UV region from 324.81 to 366.31 nm. Additionally, there are inter-CT bands from H_2O to the polyanion at 333.40 nm, and even Hopda transition absorption occurred at 340.81 nm.

The electronic absorption spectra were calculated with the number of excited states equal to 400 for POMos **2** and **3**. The simulated spectra (Fig. 2e and f) ranged from 300 to 420 nm, which is similar to the values of the experimental data (Fig. 2b and c) for **2** and **3**, respectively. The main excitations at low energy as well as suitable oscillator strength were selected for a detailed analysis of **2** and **3** (Tables S1 and S2†). The transition wavelength from the ground state to the 12th excited state (S_0–S_{12}) for **2** is 415.32 nm, with an oscillator strength of 0.00782, which were contributed by HOMO to LUMO+3 (85.6%) and HOMO−4 to LUMO (12.1%). The HOMO and LUMO+3 are mainly distributed on π orbitals within the aromatic group of H_2mpda and Mo atoms within the polyanion, respectively (Fig. 2h and Fig. S6b, c†).

The hole–electron analyses of **2** (Fig. 2k and Fig. S6d, S9†) further indicated that S_0–S_{12} is an inter-CT from H_2mpda to the polyanion. The transition wavelength from the ground state to the first excited state (S_0–S_1) in **3** is 419.75 nm, and was accompanied by an oscillator strength of 0.02069. This value was attributed to the contributions from HOMO to LUMO (99.1%). Specifically, the HOMO and LUMO dominantly reside in the π orbitals within the aromatic group of H_2ppda and the Mo atoms within the polyanion, respectively (Fig. 2i and Fig. S7b, c†). The analysis of hole–electron distributions for **3** (Fig. 2l and Fig. S7d, S10†) further suggests that the S_0–S_1 transition represents inter-CT from H_2ppda to the polyanion.

These results indicate that the absorption of **2** and **3** in the near-UV region was also attributed to inter-CT. The hole–electron overlap function S_r adequately describes the degree of overlap between the holes and electrons during an excited state. The S_r values of excited states **1** (S_0–S_2), **2** (S_0–S_{12}), and **3** (S_0–S_1) were calculated to be 0.10438, 0.18887, and 0.21163, respectively. The results show that the degree of hole–electron separation is greater for **1**, and also indicate that the hole–electron separation degree of **1** is the highest.

A comparison of the inter-CT bands for **2** and **3** indicated that the transition energy required to the near-infrared (NIR)

Table 1 List of the primary excited states for **1**

Excited state	Wavelength (nm)	Oscillator strength	Electronic transition (%)	Assignment
S_0–S_2	990.49	0.00109	HOMO → LUMO+1 (100.0%)	Hopda → Mo_8
S_0–S_{109}	621.13	0.01020	HOMO−5 → LOMO+8 (97.5%)	
S_0–S_{143}	582.93	0.01513	HOMO → LUMO+23 (95.8%)	
S_0–S_{193}	551.12	0.01061	HOMO−1 → LUMO+29 (99.8%)	
S_0–S_{248}	498.72	0.01118	HOMO−2 → LUMO+32 (99.1%)	
S_0–S_{451}	405.81	0.01118	HOMO−15 → LUMO+8 (99.7%)	
S_0–S_{821}	331.66	0.01056	HOMO−11 → LUMO+34 (98.8%)	
S_0–S_{617}	366.31	0.01342	HOMO−9 → LUMO+23 (60.4%), HOMO−8 → LUMO+25 (38.0%)	Hopda → Mo_8 Mo_8
S_0–S_{620}	365.33	0.01331	HOMO−21 → LUMO+1 (84.5%), HOMO−20 → LUMO (9.7%)	Mo_8
S_0–S_{672}	356.51	0.01124	HOMO−25 → LUMO+1 (64.8%), HOMO−8 → LUMO+31 (18.3%), HOMO−24 → LUMO (13.3%)	
S_0–S_{785}	336.85	0.01522	HOMO−26 → LUMO+3 (66.7%), HOMO−27 → LUMO+2 (9.9%), HOMO−30 → LUMO+3 (9.2%)	
S_0–S_{816}	332.18	0.01543	HOMO−21 → LUMO+5 (89.9%)	
S_0–S_{887}	324.81	0.01208	HOMO−20 → LUMO+8 (56.4%), HOMO−25 → LUMO+5 (28.5%)	
S_0–S_{806}	333.40	0.01037	HOMO−9 → LUMO+35 (83.0%), HOMO−8 → LUMO+34 (10.0%)	H_2O → Mo_8
S_0–S_{759}	340.81	0.02212	HOMO−1 → LUMO+48 (88.8%), HOMO−3 → LUMO+49 (9.3%)	Hopda

Abbreviations: HOMO, highest occupied molecular orbital; LUMO, lowest unoccupied molecular orbital.

region for **1** is lower. To explain why the inter-CT of **1** is more likely to occur, the frontier molecular orbitals of anilines were obtained. As shown in Fig. 3, the HOMO energy levels of Hopda, Hmpda, Hppda, H_2opda, H_2mpda, and H_2ppda are −10.18, −9.71, −9.65, −16.09, −16.02, and −15.98 eV, respectively. The results indicate that the HOMO of all monoprotonated phenylenediamines mostly remain on the conjugated p–π orbitals between the aromatic ring and the nonbonding electrons of nitrogen atoms, while the HOMO of diprotonated phenylenediamines is located on bonding π orbitals in the aromatic ring. Therefore, due to the higher energy of nonbonding electrons compared to bonding electrons, the HOMO energies of monoprotonated phenylenediamines are significantly higher than those of diprotonic phenylenediamines. Additionally, monoprotonated phenylenediamines are more likely to yield electrons when compared to diprotonated phenylenediamines.

These results show why the inter-CT absorption band of **1** can extend to the low-energy (NIR) region. Therefore, Hopda in **1** plays a dual role. It exhibits Brønsted basicity through protonation of aniline, and also serves as a counter-ion to polyanions. It can also exhibit Lewis basicity by providing electrons, which broadens the absorption of inter-CT to the NIR region. It can be predicted that organic amines with nonbonding electrons and stronger electron donating ability as countercations will assist in further broadening the inter-CT absorption band.

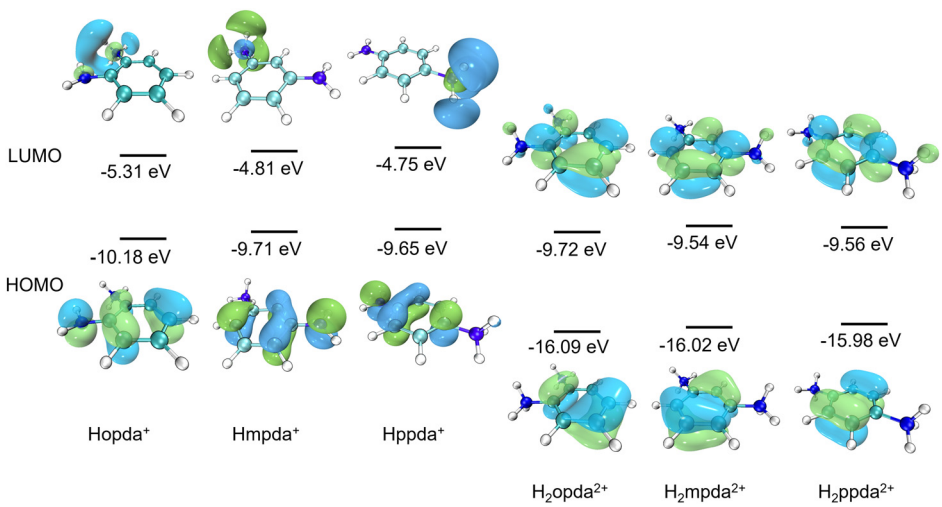

Fig. 3 Frontier molecular orbital energy levels for $Hopda^+$, $Hmpda^+$, $Hppda^+$, H_2opda^{2+}, H_2mpda^{2+}, and H_2ppda^{2+}.

In summary, three POMos with the same polyanions were synthesized to study the mechanism governing the formation of inter-CTs. POMo **1** with a strong electron donor exhibited broadening inter-CT bands from Hopda to polyanion, while POMo **2** and **3** with poor electron donors displayed inter-CT bands, which require significantly higher energy in the near-UV region. This work will inspire the design and synthesis of new optoelectronic materials with broadened absorption bands.

Conflicts of interest

There are no conflicts to declare.

Acknowledgements

This work was supported by the National Natural Science Foundation of China (22371045, 22371046), and the Fujian Natural Science Youth Innovation Project (2021J05111).

References

1 S. Shakya and I. M. Khan, Charge transfer complexes: Emerging and promising colorimetric real-time chemosensors for hazardous materials, *J. Hazard. Mater.*, 2021, **403**, 123537–112558.
2 H. L. Schläfer and G. Gliemann, *Basic Principles of Ligand Field Theory*, 1969.
3 C. Zhang, S. Peng, J. Han, C. Li, H. Zhou, H. Yu, J. Gou, C. Chen, Y. Jiang and J. Wang, Fully–Depleted $PdTe_2/WSe_2$ vander Waals Field Effect Transistor with High Light On/Off Ratio and Broadband Detection, *Adv. Funct. Mater.*, 2023, **33**, 2302466–2302475.
4 T. Chen, L. Qiu, Z. Yang, Z. Cai, J. Ren, H. Li, H. Lin, X. Sun and H. Peng, An Integrated "Energy Wire" for both Photoelectric Conversion and Energy Storage, *Angew. Chem., Int. Ed.*, 2012, **51**, 11977–11980.
5 Y. Xu, C. Li, X. Wu, M. X. Li, Y. Ma, H. Yang, Q. Zeng, J. L. Sessler and Z. X. Wang, Sheet-like 2D Manganese(IV) Complex with High Photothermal Conversion Efficiency, *J. Am. Chem. Soc.*, 2022, **144**, 18834–18843.
6 L. Xie, J. Zhang, W. Song, J. Ge, D. Li, R. Zhou, J. Zhang, X. Zhang, D. Yang, B. Tang, T. Wu and Z. Ge, Rational tuning of intermolecular and intramolecular interactions enabling high-efficiency indoor organic photovoltaics, *Nano Energy*, 2022, **99**, 107414–107426.
7 P. K. Samanta and R. Misra, Intramolecular charge transfer for optical applications, *J. Appl. Phys.*, 2023, **133**, 020901.
8 D. M. D'Alessandro and F. R. Keene, Current trends and future challenges in the experimental, theoretical and computational analysis of intervalence charge transfer (IVCT) transitions, *Chem. Soc. Rev.*, 2006, **35**, 424–440.
9 E. A. Fellows and F. R. Keene, Influence of Anions on Intervalence Charge Transfer (IVCT) in Mixed-Valence Dinuclear Complexes, *J. Phys. Chem. B*, 2007, **111**, 6667–6675.
10 M. Jiang, Y. G. Weng, Z. Y. Zhou, C. Y. Ge, Q. Y. Zhu and J. Dai, Cobalt Metal–Organic Frameworks Incorporating Redox-Active Tetrathiafulvalene Ligand: Structures and Effect of LLCT within the MOF on Photoelectrochemical Properties, *Inorg. Chem.*, 2020, **59**, 10727–10735.
11 D. M. Flores and V. A. Schmidt, Intermolecular 2 + 2 Carbonyl–Olefin Photocycloadditions Enabled by Cu(I)–Norbornene MLCT, *J. Am. Chem. Soc.*, 2019, **141**, 8741–8745.
12 X. P. Wu, L. Gagliardi and D. G. Truhlar, Cerium Metal–Organic Framework for Photocatalysis, *J. Am. Chem. Soc.*, 2018, **140**, 7904–7912.
13 W. Zhang, M. Ji, Z. Sun and K. J. Gaffney, Dynamics of Solvent-Mediated Electron Localization in Electronically Excited Hexacyanoferrate(III), *J. Am. Chem. Soc.*, 2012, **134**, 2581–2588.
14 P. Gouzerh and A. Proust, Main-Group Element, Organic, and Organometallic Derivatives of Polyoxometalates, *Chem. Rev.*, 1998, **98**, 77–112.
15 X. Zhu, L. Chen, Y. Liu and Z. Tang, Atomically precise Au nanoclusters for electrochemical hydrogen evolution catalysis: Progress and perspectives, *Polyoxometalates*, 2023, **2**, 9140031.
16 J. C. Liu, J. F. Wang, Q. Han, P. Shangguan, L. L. Liu, L. J. Chen, J. W. Zhao, C. Streb and Y. F. Song, Multicomponent Self–Assembly of a Giant Heterometallic Polyoxotungstate Supercluster with Antitumor Activity, *Angew. Chem., Int. Ed.*, 2021, **60**, 11153–11157.
17 N. Song, M. Lu, J. Liu, M. Lin, P. Shangguan, J. Wang, B. Shi and J. Zhao, A Giant Heterometallic Polyoxometalate Nanocluster for Enhanced Brain–Targeted Glioma Therapy, *Angew. Chem., Int. Ed.*, 2024, e202319700.
18 H. Wang, S. Hamanaka, Y. Nishimoto, S. Irle, T. Yokoyama, H. Yoshikawa and K. Awaga, In Operando X-ray Absorption Fine Structure Studies of Polyoxometalate Molecular Cluster Batteries: Polyoxometalates as Electron Sponges, *J. Am. Chem. Soc.*, 2012, **134**, 4918–4924.
19 D. Attanasio, M. Bonamico, V. Fares and L. Suber, Organic–inorganic charge-transfer salts based on the β-$[Mo_8O_{26}]^{4-}$ isopolyanion: synthesis, properties and X-ray structure, *J. Chem. Soc., Dalton Trans.*, 1992, 2523–2528.
20 M. A. Mohamed, S. Arnold, O. Janka, A. Quade, V. Presser and G. Kickelbick, Self–Activation of Inorganic–Organic Hybrids Derived through Continuous Synthesis of Polyoxomolybdate and para–Phenylenediamine Enables Very High Lithium–Ion Storage Capacity, *ChemSusChem*, 2023, **16**, e202202213.
21 T. Akutagawa, D. Endo, H. Imai, S. Noro, L. Cronin and T. Nakamura, Formation of p-phenylenediamine-crown ether-$[PMo_{12}O_{40}]^{4-}$ salts, *Inorg. Chem.*, 2006, **45**, 8628–8637.
22 P. Hermosilla-Ibáñez, K. Wrighton-Araneda, L. Scarpetta-Pizo, W. Cañón-Mancisidor, M. Gutierrez-Cutiño, E. Le Fur, V. Paredes-García and D. Venegas-Yazigi, The origin of the

electronic transitions of mixed valence polyoxovanadoborates $[V_{12}B_{18}O_{60}]$: from an experimental to a theoretical understanding, *New J. Chem.*, 2019, **43**, 17538–17547.

23 S. Li, Z. Zhao, T. Ma, P. Pachfule and A. Thomas, Superstructures of Organic–Polyoxometalate Co–crystals as Precursors for Hydrogen Evolution Electrocatalysts, *Angew. Chem., Int. Ed.*, 2022, **61**, e202112298.

24 K. Hakouk, O. Oms, A. Dolbecq, J. Marrot, A. Saad, P. Mialane, H. El Bekkachi, S. Jobic, P. Deniard and R. Dessapt, New photoresponsive charge-transfer spiropyran/polyoxometalate assemblies with highly tunable optical properties, *J. Mater. Chem. C*, 2014, **2**, 1628–1641.

25 D. H. Li, X. Y. Zhang, J. Q. Lv, P. W. Cai, Y. Q. Sun, C. Sun and S. T. Zheng, Photo–Activating Biomimetic Polyoxomolybdate for Boosting Oxygen Evolution in Neutral Electrolytes, *Angew. Chem., Int. Ed.*, 2023, **62**, e202312706.

26 S. Upreti and A. Ramanan, Structure-Directing Role of Hydrogen-Bonded Dimers of Phenylenediammonium Cations: Supramolecular Assemblies of Octamolybdate-Based Organic–Inorganic Hybrids, *Cryst. Growth Des.*, 2005, **5**, 1837–1843.

27 Z. Liu, T. Lu and Q. Chen, An sp-hybridized all-carboatomic ring, cyclo[18]carbon: Electronic structure, electronic spectrum, and optical nonlinearity, *Carbon*, 2020, **165**, 461–467.

28 W. Demtröder, *Laser Spectroscopy: Basic Concepts and Instrumentation*, 2003.

29 P. H. Wang, X. Y. Zhang, J. A. Fan and C. Sun, Unveiling the effect of water on photoinduced electron transfer by crystallographic study, *Chem. Commun.*, 2022, **58**, 13099–13102.